Examination of Types 308 and 308CRE Stainless Steels after Interrupted Creep Testing

The theory that the absence of a well-defined carbide network in modified Type 308 improves creep resistance is tested

BY J. M. VITEK, S. A. DAVID AND V. K. SIKKA

ABSTRACT. Interrupted creep tests were performed at 650°C on Types 308 and 308CRE (Controlled Residual Elements) material in both the homogenized and as-welded conditions. The microstructures were evaluated in order to determine the mechanism by which CRE additions, and specifically titanium additions, improve the elevated-temperature creep properties of Type 308 stainless steel. The Ti-modified Type 308 stainless steel exhibits a considerably lower steady-state creep rate, which results in a longer rupture life. In addition, the modified material has a more uniform distribution of precipitates than the unmodified alloy, and the continuous network of carbides found in the unmodified Type 308 steel along grain boundaries (homogenized material) or the ferrite/austenite interfaces (weld material) is avoided. This continuous network in the Type 308 steel provides sites for the nucleation of extensive intergranular cracks during tertiary creep.

Introduction

About 15 years ago, it was found that welds of Type 308 stainless steel made with titania- and lime-titania-covered shielded metal arc (SMA) electrodes had higher creep strength and ductility than welds made from lime-covered electrodes (Ref. 1). Later work showed that improvements in the creep behavior of Type 308 stainless steel welds may be achieved by small additions of titanium, boron and phosphorus (Refs. 2–5). Such small additions are referred to as controlled residual elements (CRE), and the modified alloy is designated Type 308CRE stainless steel. A stress-rupture plot that demonstrates the improved creep properties of Type 308CRE weld metal is shown in Fig. 1. Also included in Fig. 1 are data for the stress-rupture properties of Type 321 stainless steel, which is basically a Type 308 stainless steel with titanium additions (Ref. 6). It can be seen that in wrought stainless steels, a titanium addition improves the creep-rupture properties in the same way as CRE additions (including titanium) do in Type 308 stainless steel weld metal. Similar improvements in creep properties of wrought stainless steels resulting from boron and phosphorus, as well as titanium, additions have been found by other investigators (Refs. 7–10).

Early metallographic investigations showed that in both Types 308 and 308CRE alloy welds, elevated-temperature exposure resulted in the transformation of ferrite to sigma phase. However, creep-tested specimens of the CRE-modified steel welds did not contain internal cracks in the vicinity of the sigma phase/austenite boundaries (Ref. 3). In contrast, such cracks were common in welds of Type 308 steel subjected to elevated-temperature creep testing. However, the basis for the absence of cracks in the Type 308CRE welds, which presumably is responsible for the improvement in the creep properties, was not understood. It was suggested (Ref. 3) that the CRE additions somehow modified the sigma phase so that cracking at the sigma phase interface was avoided, but any further details as to the mechanisms involved were not given or proposed.

KEY WORDS

308 Stainless Steel
308CRE Stainless Steel
Creep Properties
Microstructure
Precipitation Behavior
GTA
Homogenized Condition
Intergranular Cracks
Fracture Behavior
Creep Ductility

An investigation was undertaken to try to understand the mechanism for the improved creep behavior of Type 308CRE weld metal. Since the improvement occurred in long-time elevated-temperature tests, the emphasis of the study was on the phase stability of these alloys as a function of elevated-temperature aging. The study was a broad-ranged effort involving several different aspects of the stability of Types 308 and 308CRE alloys. Of the three CRE additions identified as beneficial, namely titanium, phosphorus and boron, only the role of titanium was evaluated by comparing the behavior of Type 308 steel with that of a titanium-modified Type 308CRE alloy.

First, the solidification behavior of both steels was examined for several different welding conditions (Ref. 11). No significant difference was found between the two steels. The solidification mode for both alloys is that of primary ferrite formation (Refs. 11, 12). During subsequent cooling, the ferrite is unstable and transforms to austenite, as shown in the vertical section of the ternary Fe-Cr-Ni phase diagram presented in Fig. 2. The ferrite-to-austenite transformation does not proceed to completion during the cooling of Types 308 and 308CRE welds, with the result that the as-welded structure contains some residual ferrite within the primarily austenitic microstructure. Comparable quantities of residual ferrite (approximately 10%) were found in the as-solidified structures and the ferrite had

J. M. VITEK, S. A. DAVID and V. K. SIKKA are with the Metals and Ceramics Division, Oak Ridge National Laboratory, Oak Ridge, Tenn.

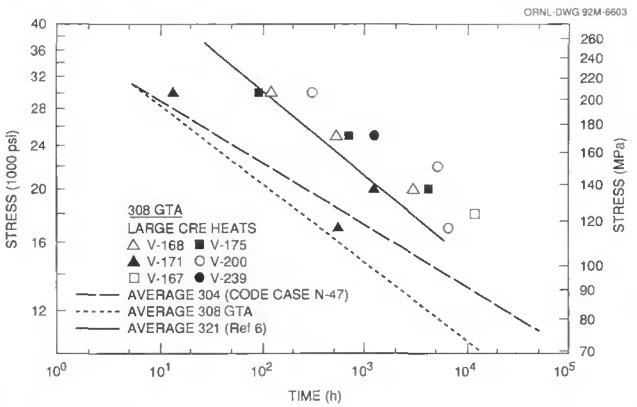

Fig. 1 — Creep-rupture stress vs. creep-rupture time at 650°C. A significant improvement in creep properties is shown for Type 308CRE steels in comparison to Types 304 or 308 steel. Data for Type 321 stainless steel are from Ref. 6.

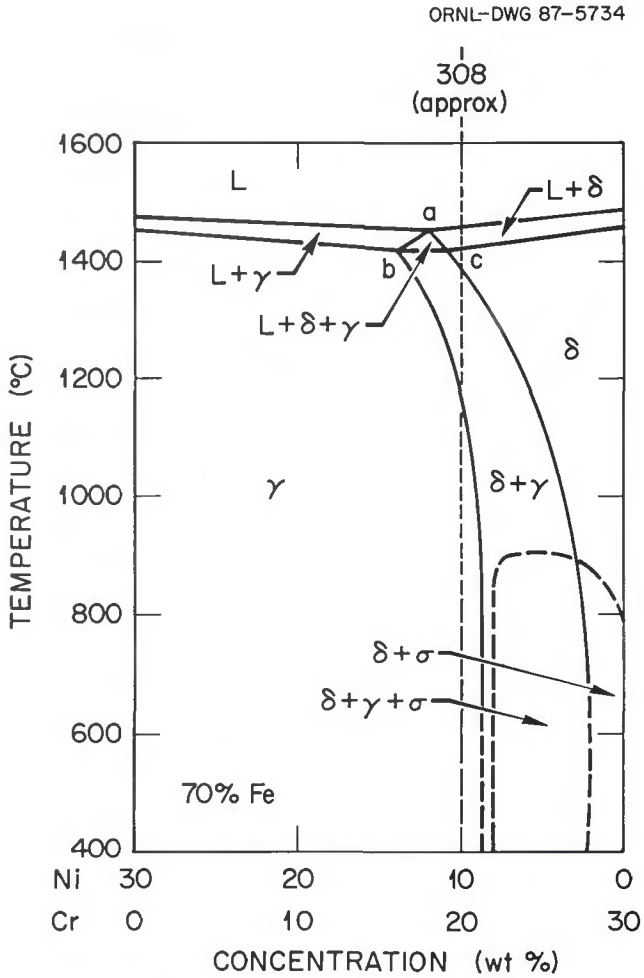

Fig. 2 — Section of the iron-chromium-nickel ternary phase diagram with the approximate location of the Type 308 stainless steel composition superimposed. Below approximately 1100°C, ferrite is not an equilibrium phase.

nearly identical morphologies for the two alloys. It was concluded that the solidification behavior could not be responsible for the improvement in creep properties (Ref. 11).

An examination of the aging behavior of Types 308 and 308CRE stainless steels was also carried out, for steels in both the as-welded (Ref. 11) and homogenized (Ref. 13) conditions. Aging temperatures from 550° to 850°C (1022°–1562°F) and aging times up to 10,000 h were examined. It was found that the titanium addition did not retard the formation of sigma phase at all. In fact, the titanium may have slightly increased the rate of formation of sigma phase during aging. However, the principal effect of the addition of titanium was to change the types of precipitates formed during aging, and to change their distribution within the duplex structure.

Table 1 — Alloy Compositions (wt-%)

Element	Homogenized Type 308	As-Welded Type 308[a]	Homogenized Type 308CRE	As-Welded Type 308CRE[a]
Cr	20.89	20.21	19.96	19.79
Ni	10.28	9.36	9.98	9.90
Mn	1.61	1.75	1.96	1.95
Si	0.49	0.46	0.62	0.61
C	0.068	0.053	0.043	0.036
S	0.012	0.008	0.015	0.014
Mo	0.05	—	<0.01	—
V	0.06	—	0.04	—
Cu	0.1	—	0.03	—
N_2	0.039	0.058	0.011	0.022
P	0.018	0.018	0.011	0.012
Ti	<0.01	<0.01	0.57	0.50
B	<0.001	0.002	0.002	0.003
Fe	balance	balance	balance	balance

(a) Average of analyses on two welds.

Rather than forming chromium-rich $M_{23}C_6$ carbides along the original ferrite/austenite interface in welded material (Ref. 11) or along the austenite grain boundaries in homogenized material (Ref. 13), titanium-rich carbides, nitrides and sulfides formed randomly throughout the matrix. It was suggested in the earlier study (Ref. 13) that the absence of a well-defined and continuous carbide network in the titanium-modified Type 308 steel may be the key to the improvement in the creep properties. The objective of the present paper was to evaluate this hypothesis by examining the microstructure of both alloys in creep specimens that were either tested to failure or interrupted at various intermediate stages of testing. In addition, the examination of shoulder and gauge sections of creep specimens that were exposed to elevated-temperatures for a range of times allowed for the evaluation of the effect of stress on the aging behavior of these alloys.

Experimental Procedure

The two alloys that were used in this study were a commercial-grade Type

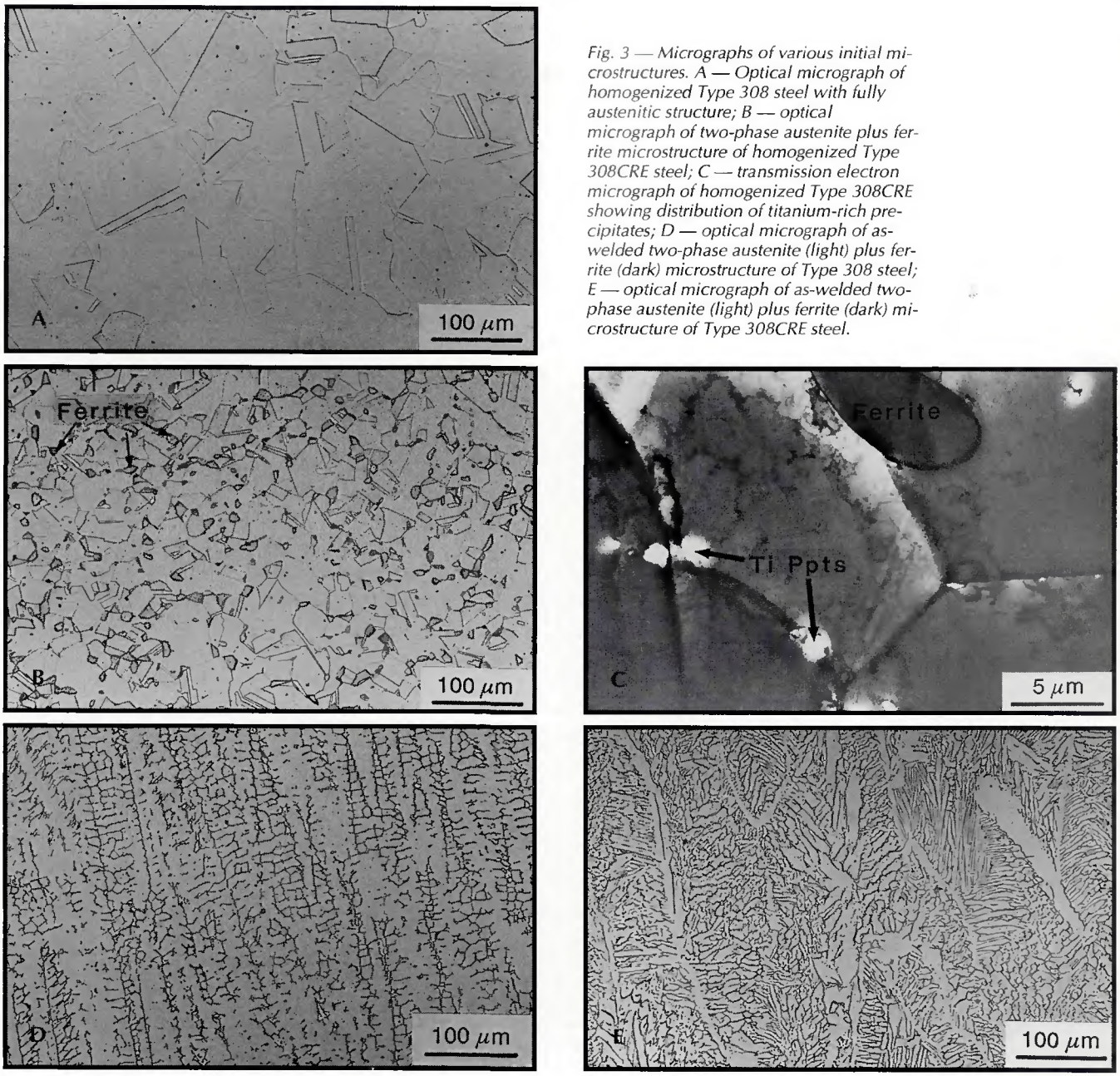

Fig. 3 — Micrographs of various initial microstructures. A — Optical micrograph of homogenized Type 308 steel with fully austenitic structure; B — optical micrograph of two-phase austenite plus ferrite microstructure of homogenized Type 308CRE steel; C — transmission electron micrograph of homogenized Type 308CRE showing distribution of titanium-rich precipitates; D — optical micrograph of as-welded two-phase austenite (light) plus ferrite (dark) microstructure of Type 308 steel; E — optical micrograph of as-welded two-phase austenite (light) plus ferrite (dark) microstructure of Type 308CRE steel.

308 stainless steel filler metal and a modified Type 308 steel with a titanium addition (referred to as Type 308CRE). The alloys were creep tested in two initial conditions, homogenized and as-welded. The homogenized material was produced by arc melting and drop casting either Type 308 or 308CRE filler metal wires into 2.5-cm (1-in.) diameter ingots and then swaging the ingots to 0.95-cm (0.37-in.) diameter rod, with two intermediate anneals at 1080°C (2156°F). The 0.95-cm-diameter rod was then homogenized at 1080°C for 1 h followed by a water quench. The as-welded samples were produced by multipass welds deposited on a 12.7-mm (0.5-in.) thick Type 304L stainless steel plate containing a single V-groove butt joint. Welds were made using the gas tungsten arc (GTA) process. Compositional analyses of the homogenized materials and representative welds are given in Table 1.

The homogenization treatment produced a fully austenitic microstructure in the Type 308 steel, while a duplex austenite plus approximately 10% ferrite microstructure was present in the Type 308CRE steel. The two-phase austenite plus ferrite microstructure could not be avoided in the homogenized Type 308CRE steel (Ref. 13). This can be readily explained by the slight compositional differences between the two alloys. If nickel and chromium equivalents (Ref. 14) are calculated, the values are 12.86 and 21.32, respectively, for the homogenized Type 308 steel and 11.43 and 21.60, respectively, for the homogenized Type 308CRE steel. Therefore, the austenite stability, which is related to the nickel equivalent, is significantly lower for the homogenized Type 308CRE steel, and thus, it was impossible to produce a fully austenitic microstructure in this alloy.

The compositional differences, at least in terms of nickel and chromium equivalents, were not as great in the as-welded materials. The nickel and chromium equivalents were 11.89 and 20.43, respectively, for the Type 308 steel weld, and 11.37 and 21.18 for the

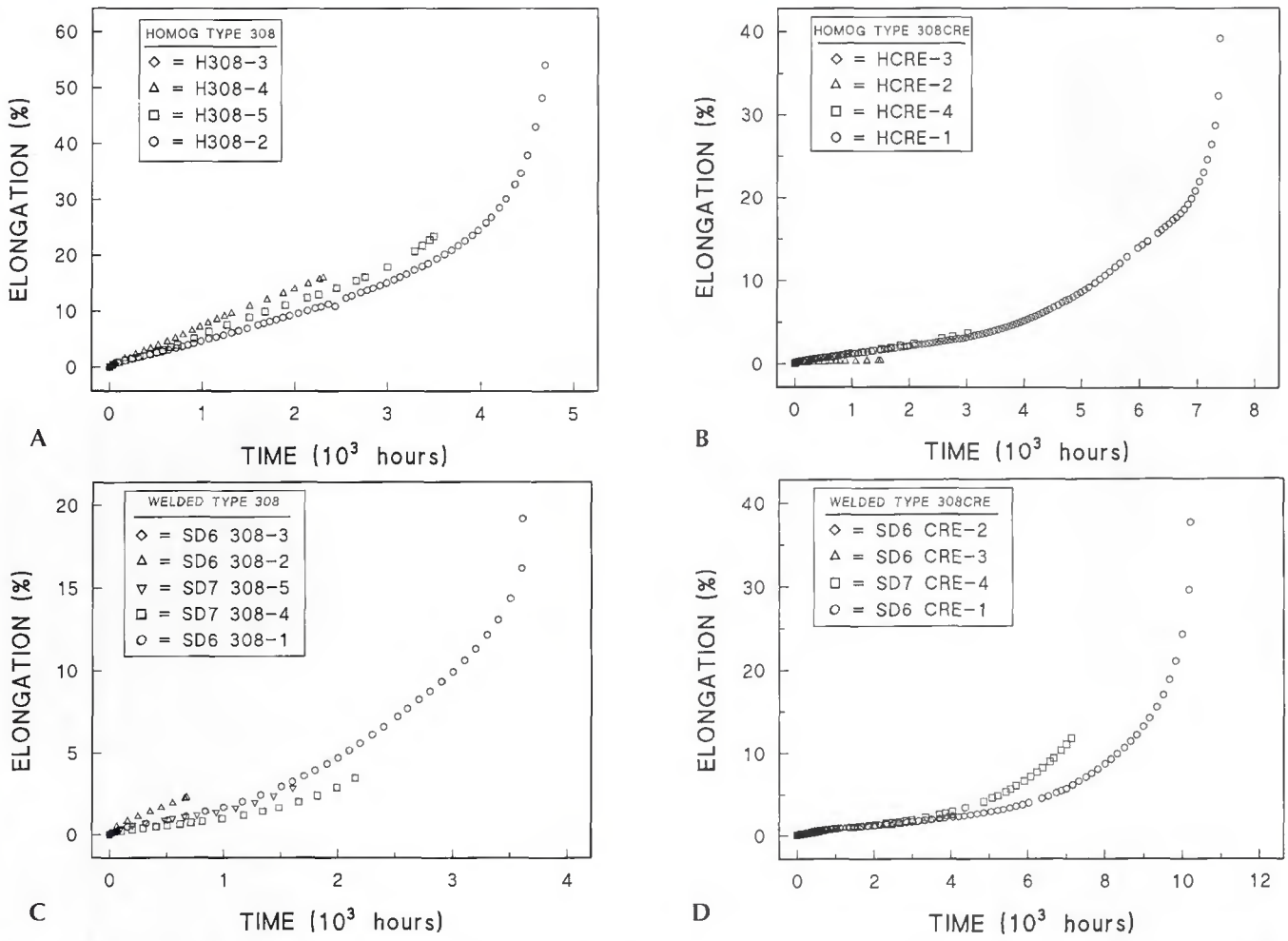

Fig. 4 — Creep curves for interrupted tests of: A — homogenized Type 308 steel; B — homogenized Type 308CRE steel; C — welded Type 308 steel; D — welded Type 308CRE steel.

Type 308CRE steel weld. The somewhat smaller nickel equivalent and larger chromium equivalent for the Type 308CRE steel weld favored ferrite stabilization and this effect was manifested by a slightly higher ferrite number (Ref. 15) in the Type 308CRE GTA weld (13.0 vs. 8.5 FN).

Creep specimens were machined from the homogenized rod and from within the welded section. Creep tests were conducted using lever arm machines. The specimens were equipped with extensometers, and measurements were taken on both sides of the specimens so that average strain readings could be taken and errors due to specimen bending or misalignment could be avoided. All tests were conducted in air at 650°C under a constant load corresponding to 16 ksi (110 MPa). Specimen temperatures were monitored throughout the test with three thermocouples attached to the gauge section. One specimen in each condition was tested to failure, and based on the measured rupture time, times were determined for other creep tests that were interrupted before failure. For the interrupted tests, specimens were cooled under load to preserve the high-temperature substructure. The actual times at temperature for all of the tests are tabulated in Table 2.

Microstructural analysis was performed by a combination of optical metallography, transmission electron microscopy, and scanning electron microscopy. Samples were prepared for optical metallography using conventional polishing techniques. Standard metallographic techniques for austenitic stainless steels were used for microstructural analysis. The metallographic samples were etched with a solution con-

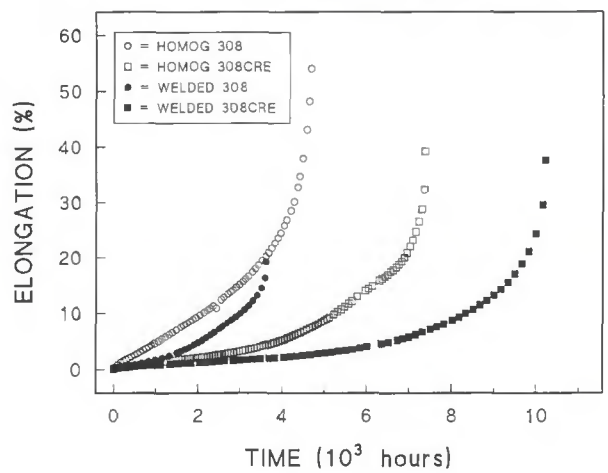

Fig. 5 — Composite of creep curves taken to failure for all four initial alloys and conditions. The creep-rupture times for the Type 308CRE steels are considerably longer than the corresponding times for the Type 308 steels.

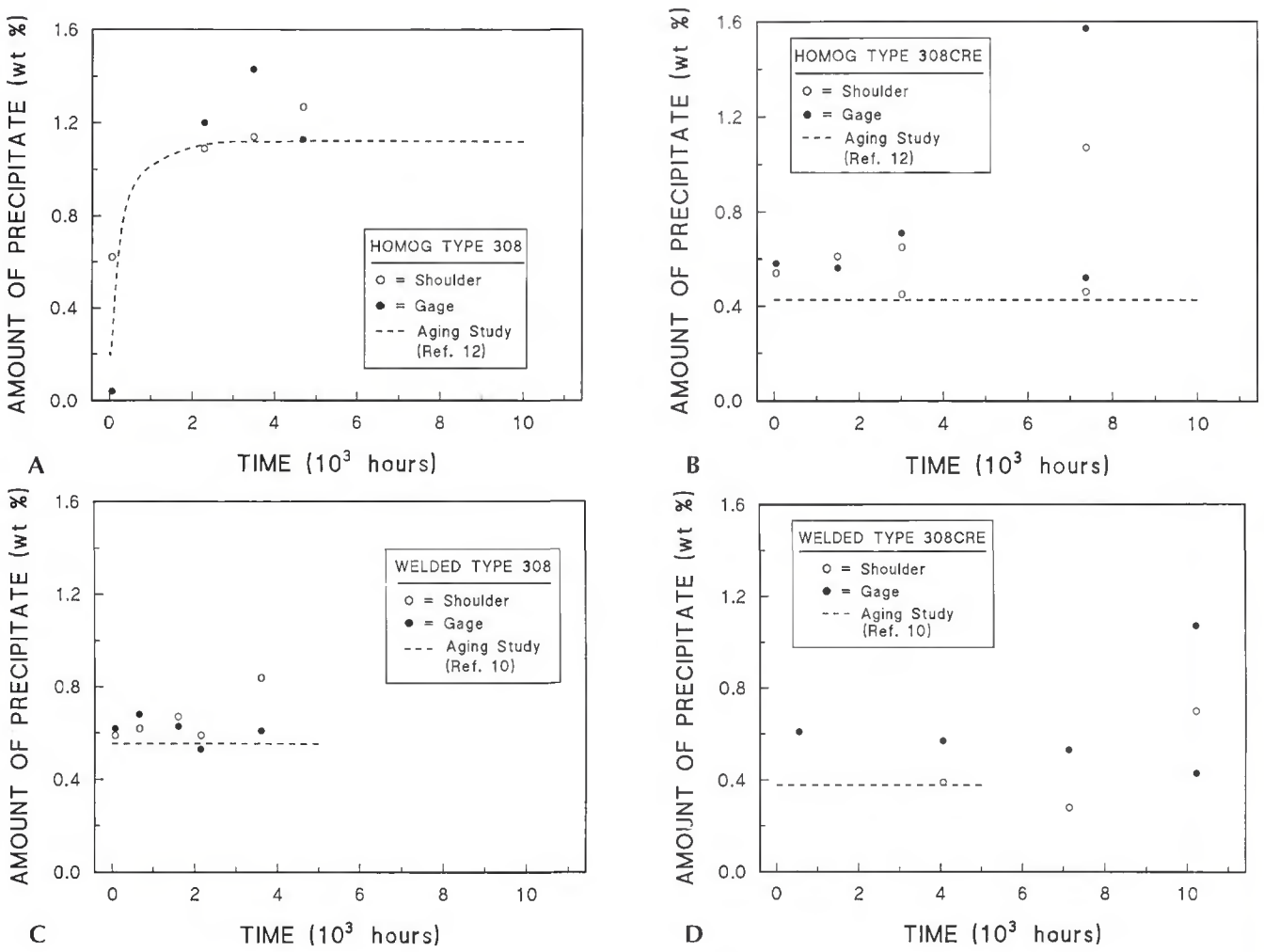

Fig. 6 — Plots of wt-% precipitate vs. test time at 650°C for: A — homogenized Type 308 steel; B — homogenized Type 308CRE steel; C — welded Type 308 steel; D — welded Type 308CRE steel. Open data points are for shoulder sections (no stress) while filled data points are for gauge sections (stressed).

taining five parts HCl and one part HNO_3. Thin foil specimens for transmission electron microscopy were made from both the stressed gauge sections of the creep specimens as well as the unstressed shoulder sections. Disks 3 mm in diameter were electrodischarge machined from wafers sliced from the bulk material. After grinding to a thickness of 0.25 mm, the disks were electrochemically polished in a dual-jet polisher in a solution of 600 mL methanol, 360 mL butyl cellusolve, and 60 mL perchloric acid. Transmission electron microscopy was carried out at a voltage of 120 kV. Limited chemical alaysis was done by energy dispersive spectroscopy on some areas examined by transmission electron microscopy. Scanning electron microscopy was performed on the metallographically-mounted ruptured specimens in the vicinity of the fracture.

The extent of precipitation that occurred during elevated-temperature exposure was determined by extraction methods. Electrolytic extractions were made on samples with an approximate mass of 0.3 g. Extractions were performed at 1.5 V for 5 h in a 10% HCl-90% methanol solution using platinum cathodes. Under these conditions, there is preferential dissolution of the austenite, ferrite, and sigma phases without affecting the precipitates that are present. The weight of the undissolved precipitates was measured in order to determine the wt-% precipitate in the original material. The reproducibility of the extraction results was determined to be ± 0.1 wt-% for the range of 0 to 4 wt-% precipitate (Ref. 16).

Results

Initial Conditions

The microstructures of the initial structures are shown in Fig. 3A–E. As noted earlier, the homogenized Type 308 steel contained a fully austenitic structure — Fig. 3A. Electron microscopy showed that the grain boundaries were free of precipitates, and electrolytic extraction results indicated that no appreciable precipitate (0.07 wt-%) was present. In contrast to the homogenized Type 308 steel, the homogenized Type 308CRE structure (Fig. 3B) was duplex austenite plus approximately 10% ferrite in the form of large isolated grains of ferrite, typically located at austenite grain boundaries. Significant precipitation was detected in the homogenized Type 308CRE steel. Small titanium-rich precipitates were found to be uniformly distributed throughout the austenite matrix — Fig. 3C. These precipitates were identified by x-ray diffraction as carbides, nitrides and sulfides. In the homogenized condition, 0.38 wt-% precipitate was present, as measured by electrolytic extractions.

The as-welded structures of both alloys were basically similar, with both containing austenite and approximately 10% ferrite — Fig. 3D and E. The ferrite was present in a highly interconnected form. The ferrite morphology in the GTA welds was primarily vermicular for the Type 308 steel, while the Type 308CRE steel contained more of an acicular fer-

Table 2 — Interrupted Creep Test Results (All Tests at 650°C, 16 ksi)

Alloy Type, Starting Condition	Specimen Identification	Time at Temperature (h)	Reduction in Area (%)	Elongation at Rupture (%)
Homogenized Type 308	H308-3	63	1.4	
	H308-4	2300	12.9	
	H308-5	3494	20.4	
	H308-2	4688(rupture)	47.3	54.1
Welded Type 308	SD6 308-3	74	0.4	
	SD6 308-2	673	2.1	
	SD7 308-5	1605	1.9	
	SD7 308-4	2154	2.3	
	SD6 308-1	3614(rupture)	33.3	19.2
Homogenized Type 308CRE	HCRE-3	50	0.1	
	HCRE-2	1498	1.5	
	HCRE-4	3021	2.8	
	HCRE-1	7382(rupture)	68.0	39.2
Welded Type 308CRE	SD6 CRE-2	550	0.7	
	SD6 CRE-3	4059	3.3	
	SD7 CRE-4	7136	12.9	
	SD6 CRE-1	10223(rupture)	60.1	37.6

rite morphology (Ref. 17). Once again, negligible precipitation was detected in the Type 308 steel in the as-welded condition (0.04 wt-%), whereas the Type 308CRE weld contained a significant amount of titanium-rich precipitates (0.13 wt-%). The precipitates in the as-welded Type 308CRE welds were uniformly distributed in the austenite matrix, as was the case for the homogenized Type 308CRE.

Creep Testing

Plots of elongation vs. test time for the interrupted creep tests for each material and each starting condition are shown in Fig. 4A–D. The specimen numbers, testing times, creep-rupture times, reduction in area, and elongations to rupture for specimens in each of the four initial conditions are given in Table 2. As shown in Fig. 4, for each of the starting conditions examined the interrupted tests followed essentially the same elongation vs. time curve as the test that was continued to rupture. For comparison of the behavior of the different alloys and conditions, a composite figure of the tests carried out to failure for the four initial conditions that were tested is presented in Fig. 5. The improvement in creep properties due to the addition of CRE elements (titanium in this case) is evident. The homogenized, and as-welded Type 308CRE materials showed significantly greater rupture lives and reductions in area. The homogenized Type 308CRE alloy showed over a 50% increase in stress-rupture life compared to the homogenized Type 308 alloy and a significant increase in reduction in area while still maintaining a large rupture elongation. The welded Type 308CRE alloy showed the longest rupture life of all the conditions tested, with nearly a 200% increase in rupture life over the welded Type 308 steel, and nearly a 100% increase in both reduction in area and rupture elongation as well. Reductions in area of over 45% and creep-rupture elongations of over 35% were found for all the materials except the as-welded Type 308 steel. Interestingly, the homogenized Type 308 stainless steel showed the greatest elongation and this was also the only material that did not contain any ferrite.

Precipitation Behavior

Electrolytic extractions were performed on both the stressed gauge sections and the unstressed shoulder sections of the creep specimens. Precipitate amount vs. the test time is plotted in Fig. 6A–D for each of the four conditions evaluated. Superimposed on the figures are dashed lines representing the extraction results from earlier aging studies on unstressed samples (Refs. 11, 13). It can be seen that in nearly all cases the new data agree well with the earlier results . Furthermore, by directly comparing the results from shoulder (unstressed) and gauge (stressed) sections, it is clear that the stress has little or no role in determining the amount of precipitate that forms upon exposure to elevated-temperatures.

The types of precipitate were not evaluated in detail. Since stress did not alter the amount of precipitate that formed, and the amount of precipitate as a function of time at elevated-temperature was similar to that found for aging without a creep stress superimposed, it was assumed the precipitates were the same as found in the earlier studies. Spot checks by electron diffraction analysis and analytical electron microscopy on a limited number of specimens confirmed this assumption. For the Type 308 stainless steel, precipitation was in the form of $M_{23}C_6$ carbides. The metallic component (M) was primarily chromium

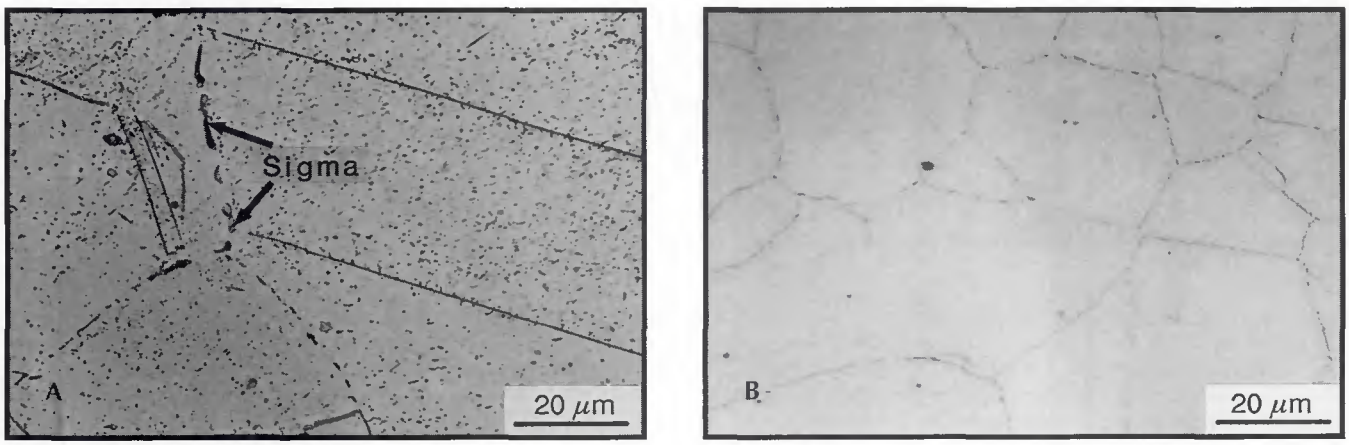

Fig. 7 — Optical micrographs of homogenized Type 308 steel. A — Extensive carbide formation along grain boundaries and within grains as well as some sigma formation in gauge section of homogenized Type 308 steel, Sample H308-5, tested for 3494 h; B — only carbide precipitation, primarily along grain boundaries, found in shoulder section of homogenized Type 308 steel, Sample H308-2, tested for 4688 h.

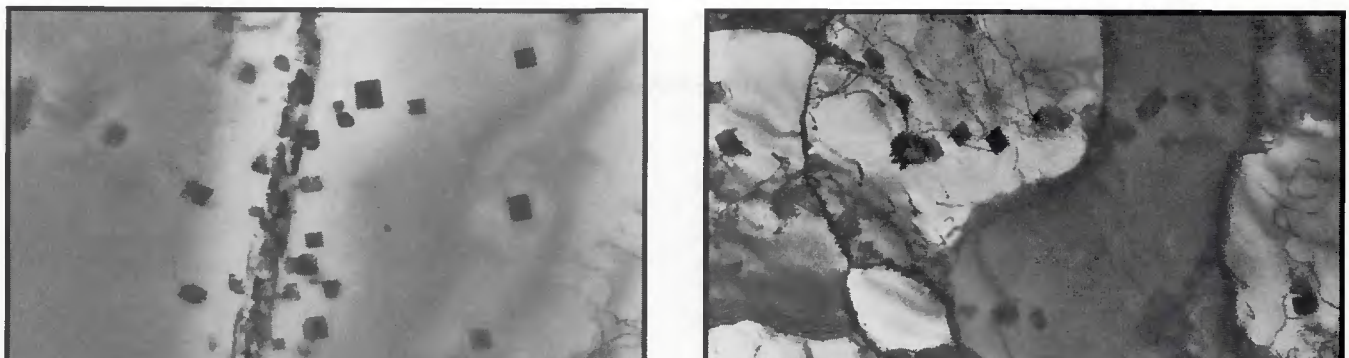

Fig. 8 — Transmission electron micrographs of homogenized Type 308 steel. A — Gauge section from Sample H3308-4, tested for 2300 h, showing carbide precipitation at grain boundaries and within the grains; B — gauge section from Sample H3308-5, tested for 3494 h and showing substructure development as well as carbide precipitation.

with some iron (Ref. 18). Precipitates in the Type 308CRE steel were titanium rich carbides, nitrides and sulfides (Refs. 11, 13).

Microstructures

Optical microscopy was performed on all of the creep-tested samples, on both the stressed gauge sections as well as the unstressed shoulder sections. However, interpretation of the microstructures was not straightforward. It was often very difficult to distinguish between ferrite and the sigma phase that formed from the ferrite. While the ferrite phase was relatively darker than the sigma phase after etching, the degree of etching affected the absolute darkness of each phase. Consequently, accurate identification was difficult when only one phase was present. When both phases coexisted, positive identification was possible by comparing the relative darkness of the etched phases. In addition, the details of the precipitation reactions were not easily followed by optical microscopy because of the limited resolution and the fine scale of the precipitates. Nonetheless, valuable information could be obtained by careful examination of the entire range of specimens and conditions, especially in terms of being able to examine large areas and evaluate the overall transformation behavior. Optical microscopy also proved to be useful in examining the microstructures of creep-ruptured samples near the fractures. Transmission electron microscopy (TEM) was utilized to provide a finer resolution of the details of the microstructural development during elevated-temperature creep testing. Finally, scanning electron microscopy (SEM) was used to examine the structures in the gauge sections of the ruptured specimens in more detail in order to evaluate better the fracture path and the mechanism of failure.

Homogenized Type 308 Steel

The microstructure of the homogenized Type 308 creep specimens showed significant precipitation along the grain boundaries after the shortest test time (Sample H308-3, 74 h). The homogenized Type 308 steel was the only alloy/condition that showed extensive grain boundary precipitation. Precipitation took place in the grain interiors after longer test times, as shown in Fig. 7. In addition, signs of sigma phase formation were evident in the gauge section after exposure for 3494 h at 650°C (1202°F) — Fig. 7A. In contrast, no sigma formation was found in the shoulder section, even after the longest exposure time of 4688 h — Fig. 7B. Of the four alloys/conditions examined, the sigma phase formation kinetics, both in the shoulder and in the gauge section, were slowest in this homogenized Type 308 steel material.

TEM examination revealed the extensive carbide formation at austenite grain boundaries as well as within the grains in homogenized and creep-tested Type 308 steel, as shown in Fig. 8A. With longer test times, a well-defined substructure was also found to have formed, as shown in Fig. 8B. The first signs of sigma phase formation were found by TEM in the gauge section of Sample H308-5, tested for 3494 h.

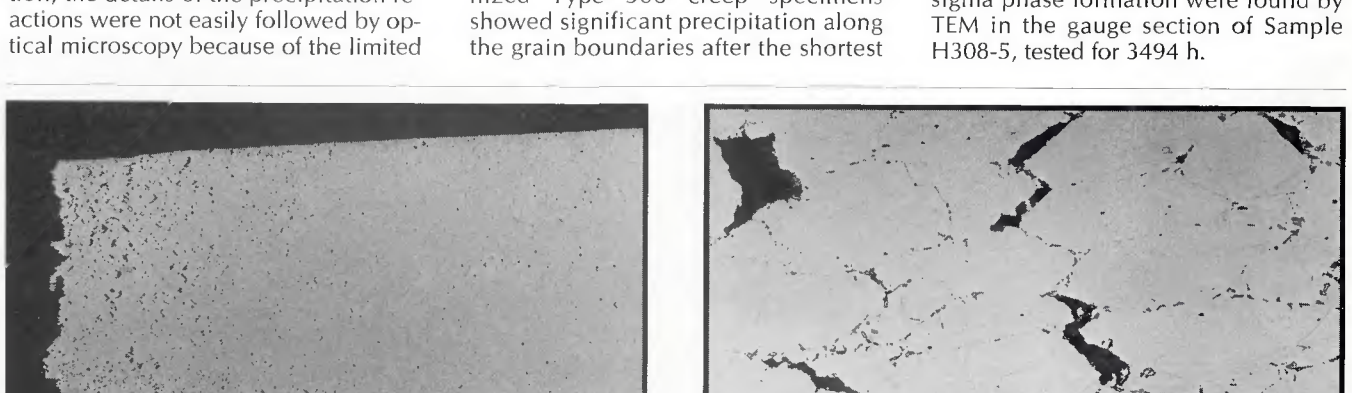

Fig. 9 — Optical micrographs near the creep-rupture fracture surface in homogenized Type 308 steel, Sample H308-2, tested for 4688 h. A — Low, and B — high magnifications showing extensive cracking. However, the exact path of the cracks cannot be determined by optical microscopy.

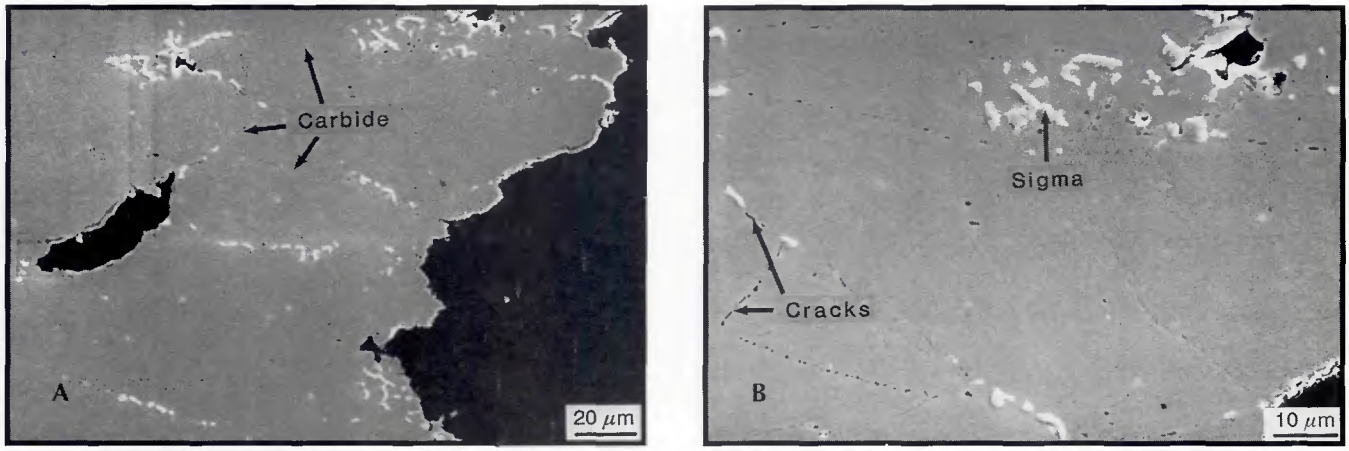

Fig. 10 —Scanning electron micrographs taken near fracture surface of homogenized Type 308 steel, Sample H308-2, tested for 4688 h. A — Low magnification view, and B — higher magnification showing cracks (dark streaks) along carbide network and not necessarily along sigma phase (light phase) boundaries.

An optical micrograph of the ruptured homogenized Type 308 stainless steel is shown in Fig. 9A. Considerable intergranular cracking was found along the gauge section of the specimen, more than was found in the welded Type 308 steel or in any of the two Type 308CRE conditions. Due to the limited resolution, optical microscopy could not reveal the exact path of the cracks. This same limitation was encountered in earlier studies (Ref. 3). For example, Fig. 9B is a higher magnification view of the homogenized Type 308 sample that was tested to rupture. It is clear that the cracking proceeded along the grain boundaries, but it cannot be determined if the cracks followed the path of the carbide precipitates or the sigma phase located at the grain boundaries. These details were resolved by SEM.

A scanning electron micrograph recorded from the immediate vicinity of the rupture surface for the homogenized Type 308 steel is shown in Fig. 10A. In this sample, which was tested to rupture (4688 h), appreciable sigma phase formation was found along the austenite grain boundaries. The sigma phase appears as the white constituent in Fig. 10A. Signs of intergranular cracking along the austenite grain boundaries, as observed by optical microscopy, were found. At a higher magnification, shown in Fig. 10B, the exact location of the cracks may be identified. A continuous dark streak that represents a small crack is found along some portions of the grain boundaries. This streak is aligned with the carbides that decorate the grain boundaries and is not associated with the sigma phase that is also present in some sections of the grain boundary.

Homogenized Type 308CRE Steel

The microstructural development in the homogenized Type 308CRE alloy was noticeably different than in the homogenized Type 308 steel. With ferrite present in the initial condition (Fig. 3B), transformation of the ferrite to sigma phase was considerably faster, being observed after only 50 h of creep testing — Fig. 11A. The same transformation behavior was found in the gauge and shoulder sections. The transformation of ferrite to sigma phase proceeded relatively quickly so that after 1498 h essentially all of the ferrite had transformed to sigma phase, as shown in Fig. 11B. No extensive precipitation along the grain boundaries, as found in the homogenized Type 308 steel, was observed in the homogenized and creep-tested Type 308CRE alloy.

Transmission electron micrographs of the homogenized and creep-tested Type 308CRE steel are shown in Fig. 12. Irregular-shaped sigma phase, the product of the ferrite to sigma transformation, is shown in Fig. 12A. The extensive carbide formation along grain boundaries that was found in the homogenized and tested Type 308 alloy was absent. However, some fine precipitation was detected in long-time tests, primarily along

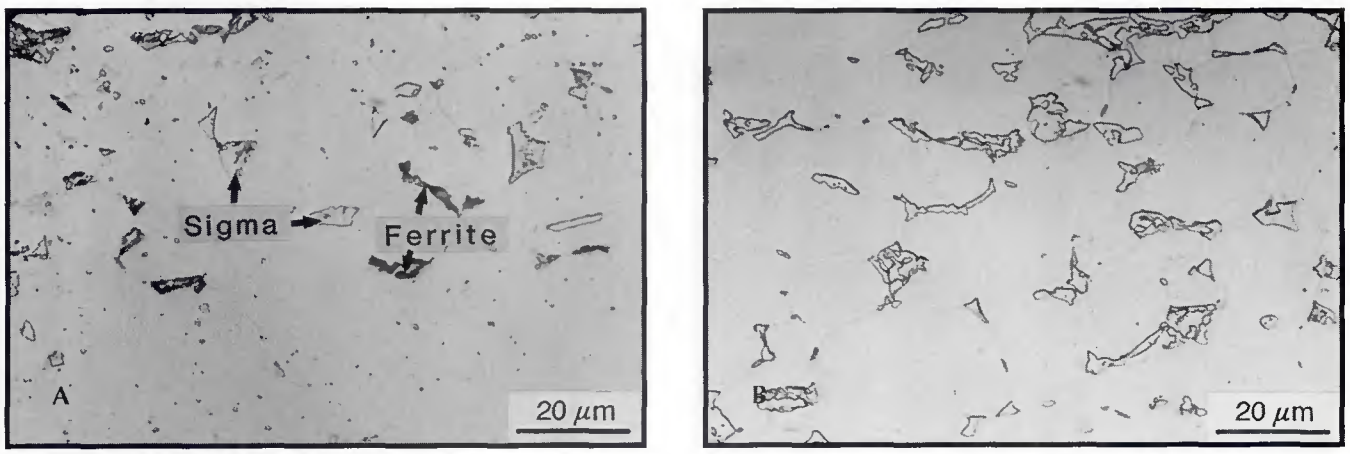

Fig. 11 — Optical micrographs of homogenized Type 308CRE steel. A — Appreciable transformation of ferrite (dark phase) to sigma phase (light phase) in gauge section of homogenized Type 308CRE, Sample H3CRE-3, tested for 50 h; B — essentially complete transformation of ferrite to sigma phase (light phase) in shoulder section of homogenized Type 308CRE steel, Sample H3CRE-2, tested for 1498 h.

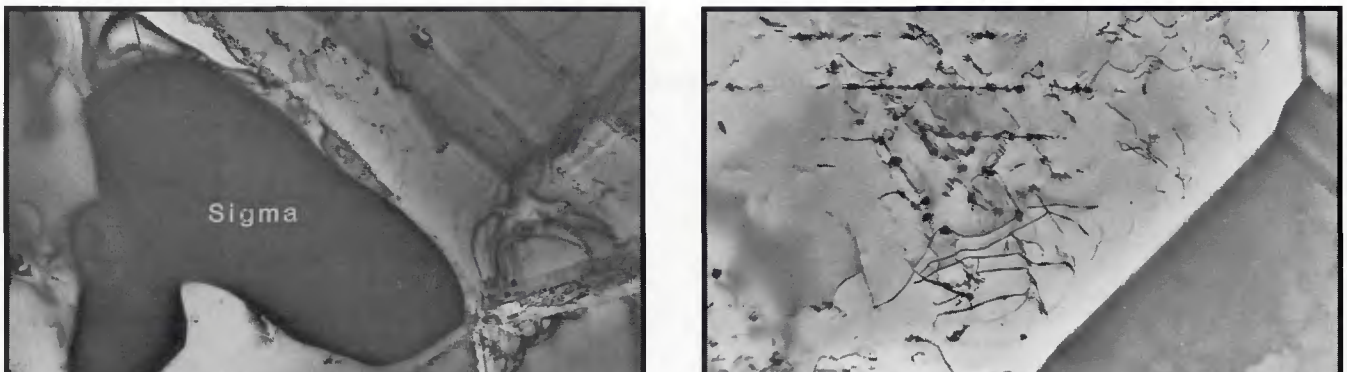

Fig. 12 — Transmission electron micrographs of homogenized Type 308CRE steel. A — Gauge section from Sample HCRE-2, tested for 1498 h, and showing sigma phase formed from ferrite; B — shoulder section from Sample HCRE-1, tested for 7382 h and showing fine precipitation along dislocations.

dislocations in the austenite grains — Fig. 12B. The majority of these precipitates were cubic TiC or TiN with a cube-on-cube orientation relation to the austenite matrix. However, some precipitates were found to contain phosphorus as well as titanium. Positive identification of these phosphorus-containing precipitates was not made.

An optical micrograph of the homogenized Type 308CRE sample tested to rupture is shown in Fig. 13A. The abundant crack formation that was found in the homogenized Type 308 steel is absent in the Type 308CRE material. The significant improvement in reduction in area compared to the homogenized Type 308 steel (Table 2) is also evident (compare Figs. 13A and 9A). A scanning electron micrograph of the homogenized and creep-tested Type 308CRE alloy is shown in Fig. 13B. Although extensive sigma phase formation along the boundaries is evident, no sign of significant intergranular cracking, as found in the unmodified homogenized Type 308 steel, was observed.

Welded Type 308 Steel

The microstructure of the welded Type 308 steel is presented in Fig. 14. After exposure at 650°C for 74 h, signs of sigma phase formation were found — Fig. 14A. Nearly 50% of the ferrite had transformed in the sample tested for 673 h. The ferrite to sigma phase transformation was essentially complete after creep testing for 1605 h — Fig. 14B. After long-term exposure and extensive transformation, the continuous nature of the residual ferrite was lost as the sigma phase formed smaller isolated islands lined up along the same directions as the longer, original ferrite fingers. Evidence of carbide formation along the original ferrite network was also found (Fig. 14B), but the carbide was barely visible in optical microscopy. The shoulder microstructure was basically identical to that found in the gauge sections.

Transmission electron micrographs of the welded and creep-tested Type 308 alloy are shown in Fig. 15. Extensive carbide formation along the original ferrite/austenite interfaces is apparent. This carbide formed a relatively continuous network throughout the material since the ferrite was originally in the form of a well-connected network — Fig. 3D. In addition to the carbide formation, recession of the ferrite/austenite boundary due to the transformation of ferrite to austenite (Ref. 19) is also evident in Fig. 15. The presence of sigma phase was first detected by electron microscopy in the sample creep-tested for 673 h, with approximately 50% of the ferrite still remaining untransformed. The limited sigma phase that was found by optical microscopy in the sample tested for only 74 h was not observed by electron microscopy, presumably because of the limited area that is examined by electron microscopy.

An optical micrograph of the welded Type 308 steel tested to rupture is shown in Fig. 16A. As with the homogenized Type 308 steel, the welded Type 308 material showed crack formation in the gauge section near the fracture surface, although to a lesser degree. Details of

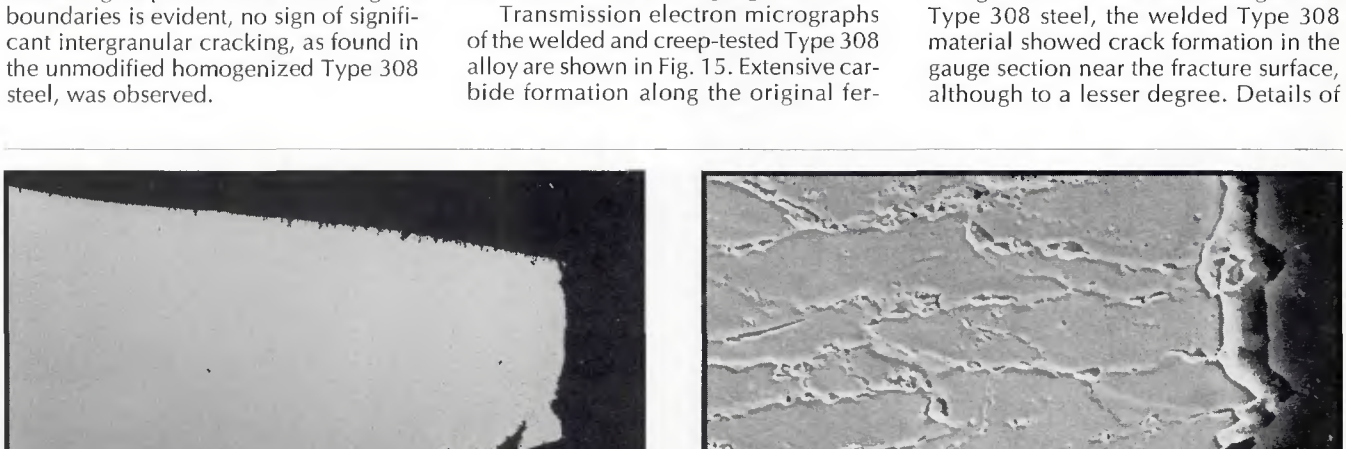

Fig. 13 — Microstructure near the fracture surface in homogenized Type 308CRE steel, Sample H3CRE-1, tested for 7382 h. Cracking is noticeably absent. A — Optical micrograph; B — scanning electron micrograph.

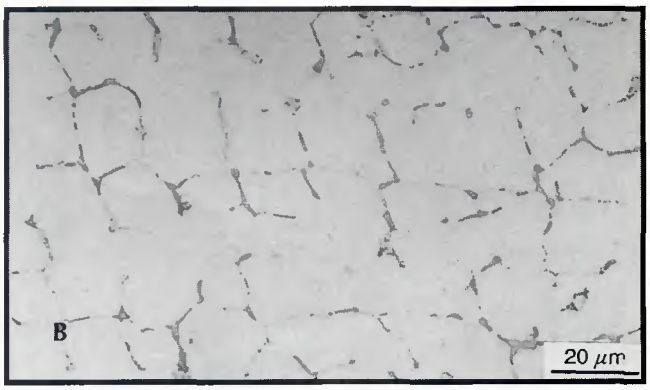

Fig. 14 — Optical micrographs of welded Type 308 steel. A — Early stages of sigma phase formation (light phase) from ferrite (dark phase) in gauge section of welded Type 308 steel, Sample SD6 308-3, tested for 74 h; B — nearly complete transformation of ferrite to sigma phase in gauge section of welded Type 308 steel, Sample SD7 308-5, tested for 1605 h.

Fig. 15 — Transmission electron micrograph of welded Type 308 steel showing extensive carbide formation along original ferrite/austenite boundary and recession of ferrite boundary prior to transformation to sigma phase. Gauge section of Sample SD6 308-2, tested for 673 h.

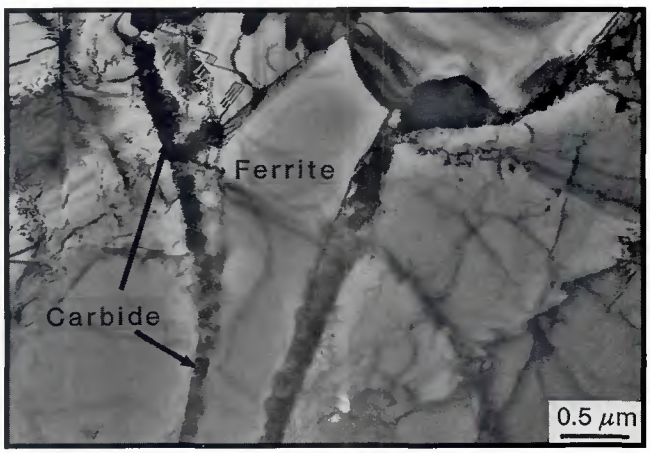

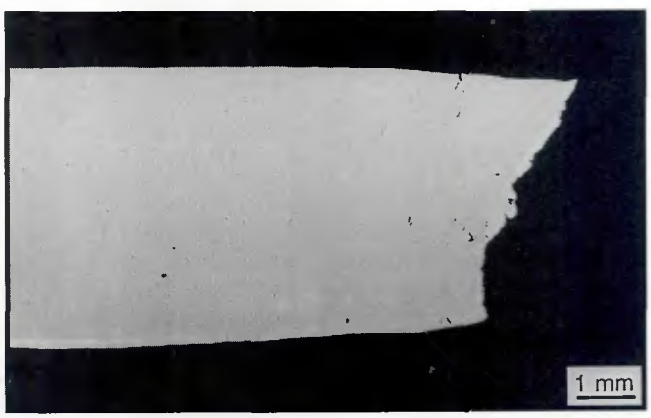

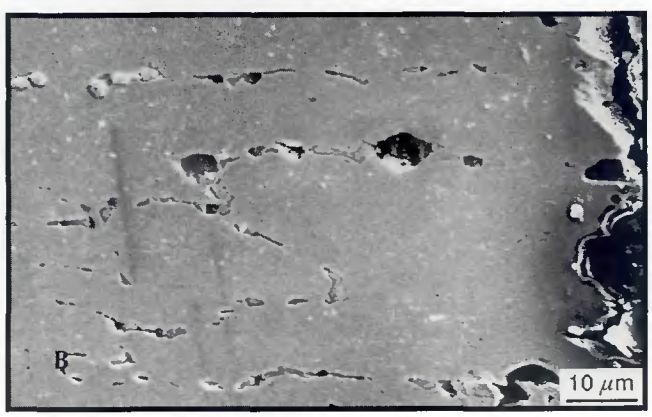

Fig. 16 — Microstructure near the fracture surface in welded Type 308 steel, Sample SD6 308-1, tested for 3614 h. A — Optical; B — scanning electron micrographs showing cracks, and C — higher magnification scanning electron micrograph showing the path of the cracks is along the carbide precipitate network and not along the sigma phase boundaries.

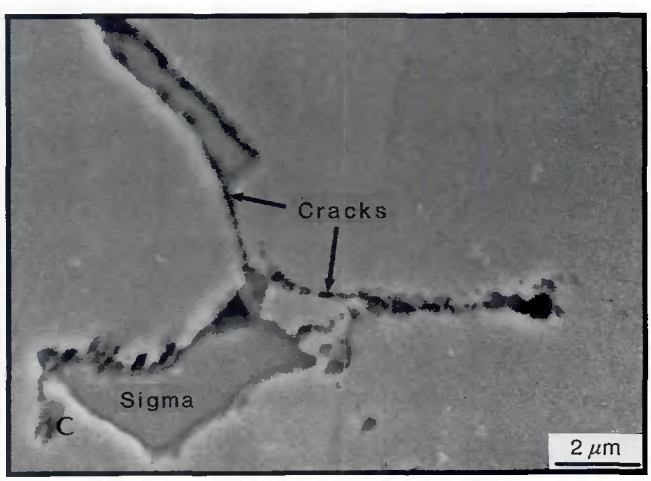

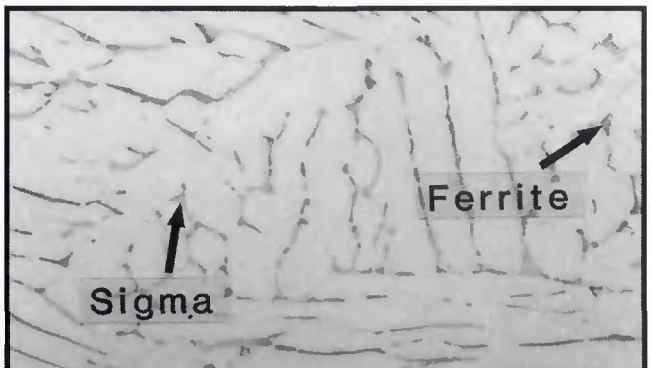

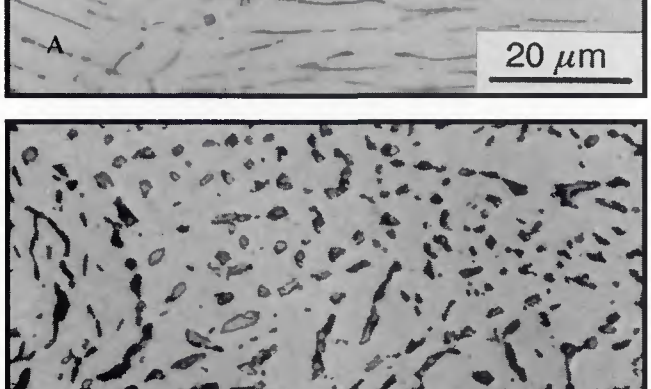

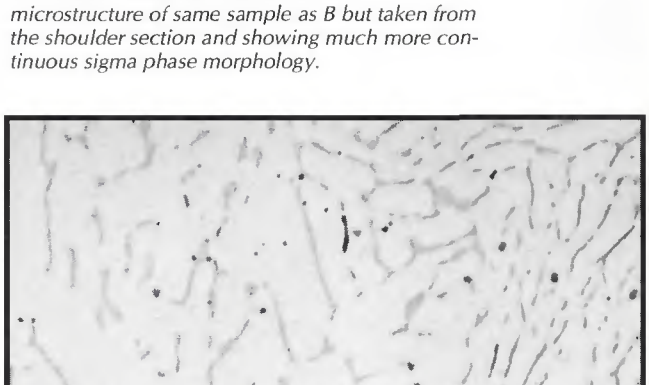

Fig. 17 — Optical micrographs of welded Type 308CRE steel. A — Later stages of ferrite (dark phase) to sigma (lighter phase) transformation in gauge section of welded Type 308CRE, Sample SD6 CRE-2, tested for 550 h; B — breakup of sigma phase structure after longer term testing. Gauge section of welded Type 308CRE, Sample SD6 CRE-1, tested for 10223 h; C — microstructure of same sample as B but taken from the shoulder section and showing much more continuous sigma phase morphology.

the nature of the crack path are provided by scanning electron micrographs, shown in Fig. 16B and C. At the higher magnification shown in Fig. 16C, the cracks are seen to follow the network of carbides which outlines the original ferrite/austenite interface. In most cases, this network is removed from the sigma phase/austenite boundary since the ferrite boundary recedes to a limited extent before transforming to sigma phase. In some instances, where the ferrite boundary did not move before sigma phase formation, the cracks along the carbide network also lie along the sigma phase/austenite interface.

Welded Type 308CRE Steel

The final condition that was examined was the welded Type 308CRE, and the microstructures are presented in Fig. 17. As seen in Fig. 17A, nearly all of the ferrite had transformed to sigma phase after 550 h. As was observed in the welded Type 308 alloy, there was a tendency for the continuous ferrite to break up into smaller islands of sigma phase upon transformation. No appreciable precipitation during creep-testing was observed. The breakdown of the continuous second phase network was quite dramatic after longer creep testing times, as shown in Fig. 17B. Figure 17B also demonstrates the difficulty in distinguishing the ferrite and sigma phases when only one of these phases is present in the microstructure. Although the second phase appears to be dark, and therefore may be an indication of ferrite, electron microscopy confirmed that the second phase by optical microscopy was sigma. It is possible that the distinction between ferrite and sigma phase is more difficult in the welded Type 308CRE material because the second phase is finer than in the Type 308 weld. As was the case for the welded Type 308 and the homogenized Type 308CRE, there was little difference in the microstructures of the gauge and shoulder sections. The only noticeable difference was that the breakdown of the continuous second phase network was less significant in the shoulder section, as shown in Fig. 17C.

TEM examination revealed that the welded and creep-tested Type 308CRE material showed extensive transformation of ferrite to sigma phase, even in the sample from the shortest creep test, SD6 CRE-2, tested for 550 h. After longer testing times, the sigma phase was found to have broken up considerably (Fig. 18A and B), and therefore, the initial narrow and interconnected ferrite morphology present in the as-welded condition was lost. As found in the homogenized Type 308CRE material, a very fine precipitate in the austenite matrix was observed in aged Type 308CRE welds — Fig. 18C. Such fine precipitation was detected in the short-time as well as long-term aged samples. The majority of these precipitates were found to be cubic titanium carbides or nitrides (a_o = 0.424 nm). Some additional precipitates that were rich in both titanium and phosphorus were also found but positive identification of these precipitates was not made.

An optical micrograph of the area near the fracture for the Type 308CRE weld is presented in Fig. 19A. As observed for the homogenized Type 308CRE material, little crack formation was observed, and the improved reduction in area (Table 2), compared to the Type 308 weld, is evident. A scanning electron micrograph of the welded and creep-tested Type 308CRE structure is shown in Fig. 19B. Very limited cracking was found, although extensive sigma phase was detected. Without the presence of a well-defined carbide network, fine crack formation is found within the

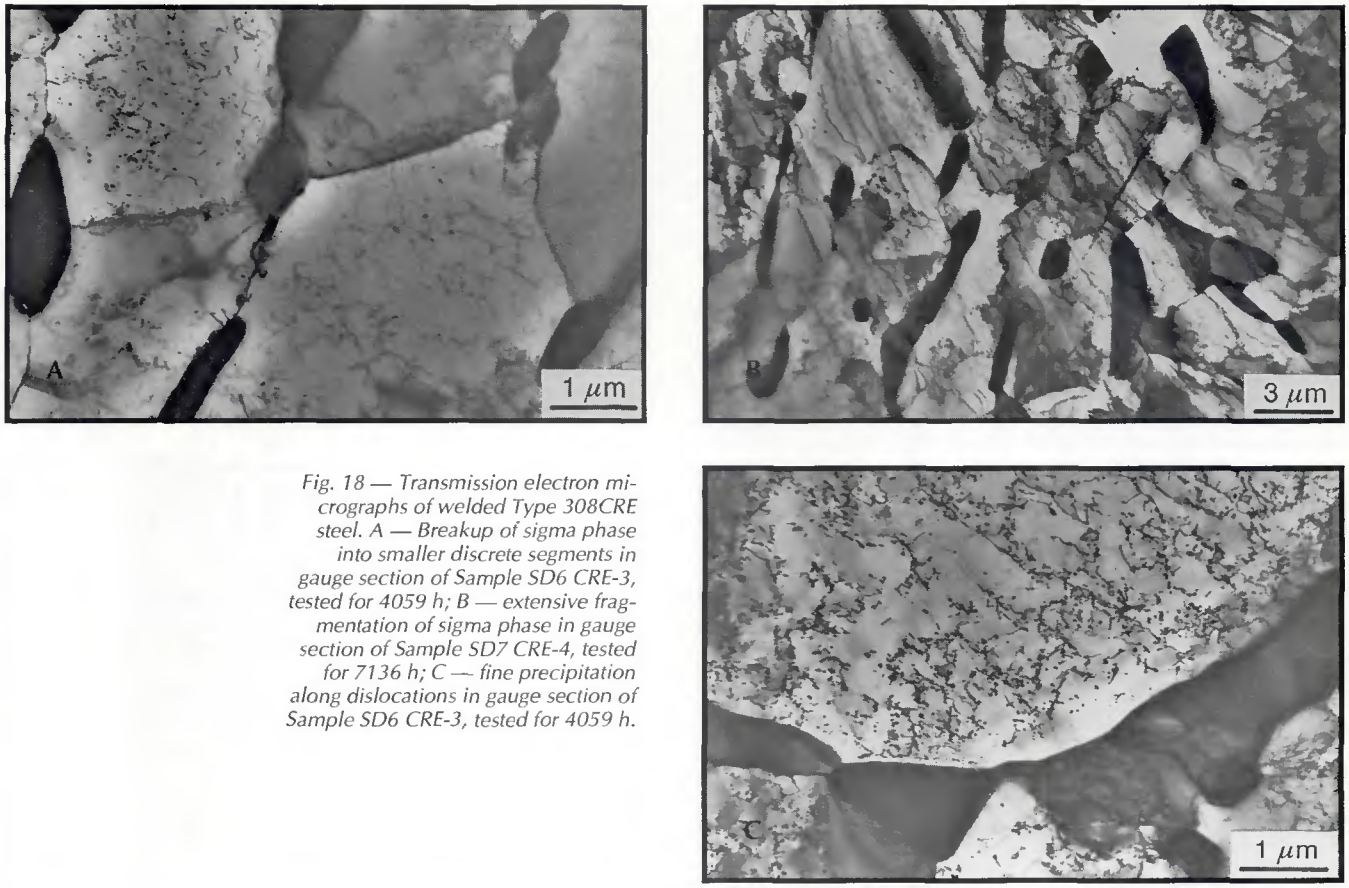

Fig. 18 — Transmission electron micrographs of welded Type 308CRE steel. A — Breakup of sigma phase into smaller discrete segments in gauge section of Sample SD6 CRE-3, tested for 4059 h; B — extensive fragmentation of sigma phase in gauge section of Sample SD7 CRE-4, tested for 7136 h; C — fine precipitation along dislocations in gauge section of Sample SD6 CRE-3, tested for 4059 h.

second most vulnerable location, namely, within the sigma phase, as shown in Fig. 19C.

Discussion

The present results on the microstructural changes during elevated-temperature creep testing are in excellent agreement with earlier results on the aging behavior of the same alloys but without any applied stress (Refs. 11, 13). It was found earlier that the primary difference in the aging behavior between the Types 308 and 308CRE alloys was the type and distribution of precipitate that was formed. For the Type 308 steel, carbide precipitation during exposure to elevated-temperatures is extensive, with preferential formation along austenite grain boundaries in the homogenized condition and along austenite/ferrite interfaces in the welded material. The net result is the formation of a highly connected network of carbides throughout the matrix. In contrast, the Type 308CRE alloy forms titanium-rich precipitates (carbides, nitrides, sulfides) that are randomly distributed in the matrix without any preferential sites and without the formation of a continuous grain boundary precipitate network. The present study found the same effects during aging in the presence of stress (creep testing), indicating that stress had no influence on the type or distribution of precipitate that formed.

It was proposed in the earlier aging studies (Refs. 11, 13) that the beneficial influence of CRE additions, and in particular the titanium addition, is in the change in the type of precipitation and its distribution. Without titanium additions, short-term exposure to elevated-temperatures produces a continuous network of carbides, and it was proposed that this network provided an easy path for crack formation and/or propagation. The present results show that the basis for the improved creep properties is more involved than simply the elimination of a continuous network of carbides in the CRE materials. Figure 5 clearly shows that the steady-state creep rate in the CRE-modified alloy is lower, and this is likely associated with higher strength properties of the CRE material. As a result of the higher yield strength of homogenized or welded 308CRE, the 16 ksi load that was used was a smaller fraction of the yield strength and the CRE material was effectively loaded to a less severe degree. The lower effective load led to a lower steady-state creep rate and therefore a longer rupture life.

The source of the improvement in strength is not exactly known. Three possible factors may combine to improve the strength. First, the more uniform precipitation may be beneficial. Second, the presence of ferrite in the homogenized CRE material may improve the strength. The homogenized 308 contains no ferrite. In the case of the welds, the CRE material contains slightly more ferrite. Finally, in the welds, the ferrite distribution is somewhat finer in the CRE material and this may enhance the strength properties of this material.

In addition to the higher steady-state creep rate that is found for the Type 308 steel, the extensive cracking that was observed in the Type 308 material plays a role in limiting the third stage of creep, beyond the steady-state creep stage. In the third stage, cracks will nucleate and propagate and the propensity of the Type 308 material to form cracks along the carbide network will shorten this stage as well. The carbide network also leads to a loss in the ductility as measured by the reduction in area (RA). The RA is a more reliable and accurate indicator of the intrinsic material ductility than total ductility. The modified alloy has a significantly larger RA than the unmodified material (Table 2), and this improvement in ductility is a result of the Ti-modified alloy's ability to resist the formation of

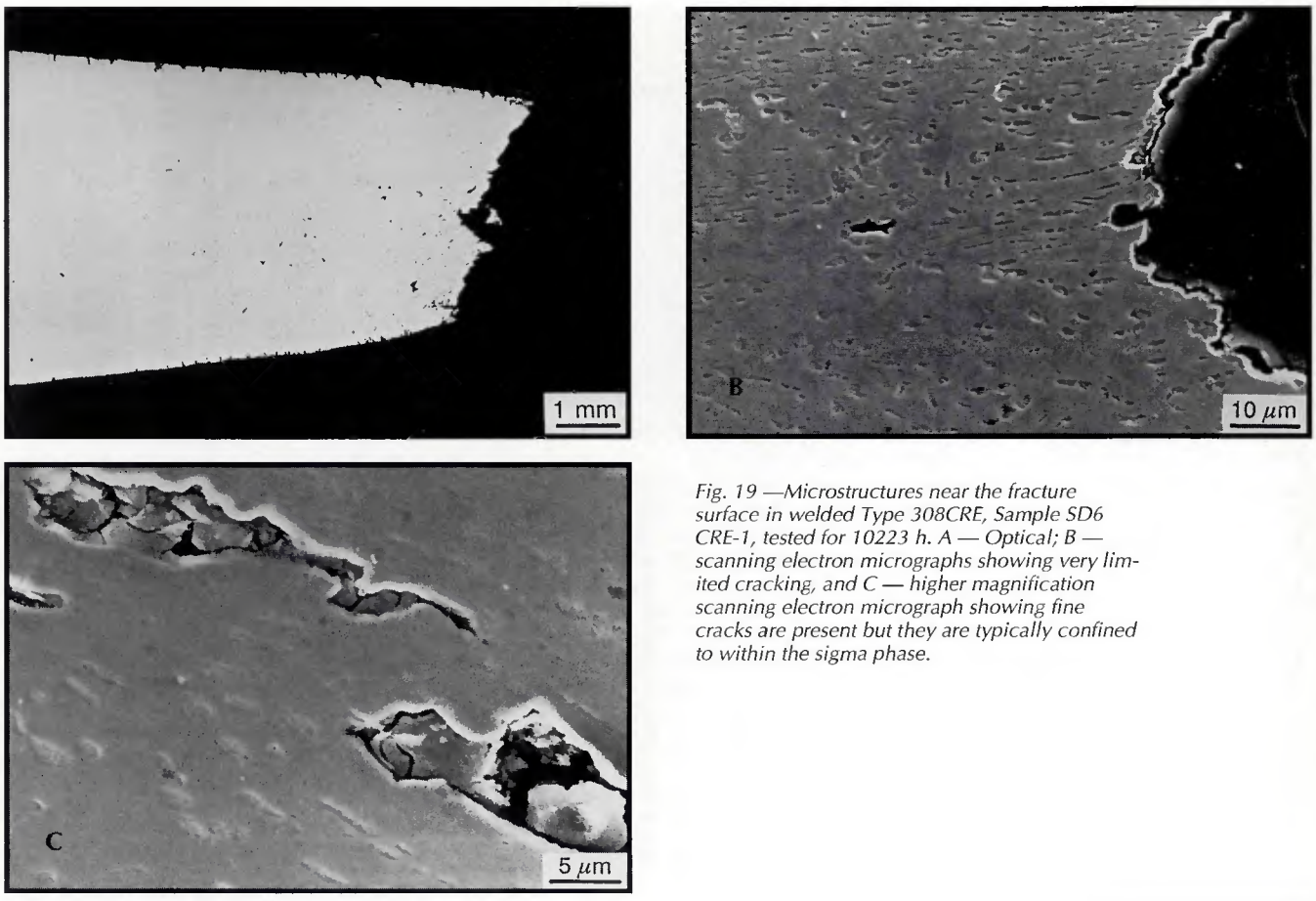

Fig. 19 —Microstructures near the fracture surface in welded Type 308CRE, Sample SD6 CRE-1, tested for 10223 h. A — Optical; B — scanning electron micrographs showing very limited cracking, and C — higher magnification scanning electron micrograph showing fine cracks are present but they are typically confined to within the sigma phase.

intergranular cracks that are found in the unmodified Type 308 steel.

The detrimental effect of carbide precipitation has been noted before for Type 316 weld metal (Ref. 20). The effect of a carbide network may be more pronounced at the relatively low stresses that were examined in the present work, since intergranular failure becomes more likely at low stresses (Ref. 21). Several other observations of cracking along the ferrite/austenite interface in welded stainless steels have been made (Refs. 22, 23). Unfortunately, these studies did not distinguish between cracking at the actual ferrite (sigma)/austenite interface or in the immediate vicinity of this interface where precipitation of a carbide network such as found in the present study is expected. It has been suggested (Ref. 22) that the elimination of a continuous ferrite network will improve creep properties. The results of the present investigation indicate that such removal of a continuous ferrite network is indeed desirable because it eliminates the development of a continuous carbide network during elevated-temperature exposure.

When carbide networks are absent, cracks were found within the sigma phase — Fig. 19C. This is not surprising, considering the brittle nature of sigma phase and its traditional association with embrittlement. However, it is important to note that the brittleness of the sigma phase is only of secondary importance when an interconnected carbide network is also present. The primary importance of the carbide network (rather than sigma phase) in affecting crack formation and creep rupture behavior is also demonstrated by the fact that the homogenized Type 308 material showed the greatest cracking, and yet sigma phase formation in this material was the most sluggish, since ferrite was absent in the initial microstructure.

Sigma phase formation kinetics were rapid in all three conditions in which ferrite was present in the initial microstructure. In the one case in which ferrite was not present (homogenized Type 308), the development of sigma phase was very sluggish. The effect of ferrite in hastening sigma phase formation has been well documented, and the details of the transformation have been described elsewhere (Ref. 24). The same mechanism appears to take place during elevated-temperature creep testing. The ferrite interface recedes initially as the ferrite becomes enriched in chromium and depleted in nickel, and then the ferrite transforms to sigma phase. The recession of the ferrite interface is particularly noticeable in the welded Type 308 samples, where carbide decorates the original ferrite/austenite interface — Fig. 15.

The kinetics of the sigma phase formation during creep testing can be compared with TTT (time-temperature-transformation) diagrams developed for aging of these alloys in the absence of stress (Refs. 11, 13). For the three conditions in which ferrite was initially present in the microstructure, the times for the onset, and completion, of the ferrite to sigma transformation are in excellent agreement with such TTT diagrams. Unfortunately, it is impossible to evaluate exactly how the precipitation kinetics compare with the earlier results on unstressed samples since the increments in exposure time were far too large in the present study. The kinetics of sigma formation in creep-tested homogenized Type 308 differ somewhat from the earlier results, indicating that an effect of stress exists, as described below. All of the present results regarding sigma phase formation are in agreement with the nucleation-limited transformation model that was described elsewhere (Ref. 24).

The effect of stress on the microstruc-

tural stability was, in general, negligible. As shown in Fig. 6, there was essentially no difference in the amount of precipitate that formed in the stressed or unstressed sections of the creep samples. There was also no evidence that stress influenced the type or distribution of the precipitates. For those alloys that initially contained ferrite, and in which the transformation of ferrite to sigma phase was relatively rapid, again, stress had little effect on the sigma phase formation kinetics; the shoulder and gauge sections had essentially identical microstructures. However, a significant effect of stress was noticed in the homogenized Type 308 alloy. In the unstressed regions, the formation of sigma phase was very sluggish. No sigma phase was found in the longest aged specimen available (4648 h). The results are in agreement with earlier work showing sigma phase first appears after 10,000 h of aging at 650°C. In contrast, the stressed gauge sections showed enhanced sigma formation kinetics, with sigma present after aging 3500 h. This influence of stress on sigma phase formation is well documented (Ref. 24). Thus, although important in only limited conditions, the effect of stress must be taken into account when applying aging study results to conditions where stress is present. Finally, stress had an effect on the distribution of the sigma phase in the long-term tests. Apparently, creep deformation broke up the sigma phase (or ferrite prior to transformation of sigma) so that the characteristic distribution of the ferrite phase in the welded samples, reasonably retained by the sigma phase during aging without stress, was disrupted and slowly disappeared.

Summary and Conclusion

The microstructures of Types 308 and 308CRE stainless steel were examined after creep testing at 650°C for various times up to and including the rupture time. The alloys were examined in both the homogenized and as-welded conditions. Based upon the results, the following conclusions were made:

1) The precipitation behavior was unaffected by the presence of the creep stress during elevated-temperature exposure. The types of precipitate and the precipitate distributions were the same as found in earlier studies in the absence of stress.

2) The Ti-modified Type 308CRE steel showed a significantly lower steady -state creep rate, which led to a large increase in the rupture life. This is attributed to the higher strength of the modified alloy, which results in a relatively lower load (and lower creep rate) than that for the Type 308 steel.

3) Extensive intergranular cracking was found in the homogenized Type 308 steel and to a lesser degree in the as-welded Type 308 steel. This cracking was found to follow the nearly continuous network of carbides that formed along austenite grain boundaries (homogenized) or ferrite/austenite interfaces (as-welded). Such precipitate networks and the associated cracking were not found in the Type 308CRE steel.

4) The absence of extensive intergranular cracking in the Type 308CRE steel, in both the homogenized and as-welded conditions, leads to improved creep ductility as measured by the reduction in area.

5) The presence of a stress during elevated-temperature exposure did not influence the kinetics of the ferrite to sigma transformation. However, in the homogenized Type 308 steel, which did not contain ferrite in the initial microstructure, the kinetics of sigma phase formation were significantly enhanced by the presence of a stress.

6) In the Type 308CRE steels, in which continuous networks of carbides were absent, small cracks were found within the sigma phase. However, this cracking did not extend beyond the boundaries of the sigma phase and did not lead to large-scale cracking in the matrix.

Acknowledgments

The authors would like to acknowledge the technical support provided by K. F. Russell, C. P. Haltom, J. W. Jones, and R. W. Reed. Their assistance in specimen preparation and electrolytic extraction measurements is appreciated. H. D. Upton is acknowledged for performing the creep tests. R. L. Klueh and E. P George are thanked for their comments in reviewing the manuscript. This research was sponsored by the Division of Materials Sciences, U.S. Department of Energy, under contract DE-AC05-84OR21400 with Martin Marietta Energy Systems, Inc.

References

1. Binkley, N. C., Berggren, R. G., and Goodwin, G. M. 1974. Effects of slight compositional variation on Type E308 electrode deposits. *Welding Journal* 53(2): 915 - 955.

2. King, R. T., Stiegler, J. O., and Goodwin, G. M. 1974. Relation between mechanical properties and microstructure in CRE Type 308 weldments. *Welding Journal* 53(7):307-s to 313-s.

3. Stiegler, J. O., King, R. T., and Goodwin, G. M. 1975. Effect of residual elements on fracture characteristics and creep ductility of Type 308 stainless steel weld metal. J *Eng. Mater. Technol.* 97(3):245–250.

4. Klueh, R. L., and Edmonds, D. P. 1986. Chemical composition effects on the creep strength of Type 308 stainless steel weld metal. *Welding Journal* 65(1):1-s to 7-s.

5. Klueh, R. L., and Edmonds, D. P. 1986. Chemical composition effects on the creep of Type 316 and 16-8-2 stainless steel weld metal. *Welding Journal* 65(6):156-s to 162-s.

6. *Aerospace Structural Metal Handbook*, Wolf, J. and Brown, W. F., Jr., eds., Belfour Stulen, Inc., Traverse City, Michigan, 1973.

7. Williams, T. M., Harries, D. R., and Furnival, J. 1972. Creep-rupture behavior of Type 316 austenitic steel in relation to boron content. J Iron Steel Inst. 210:351–358.

8. Ceccarelli, M., Santucci, R., and Bennani, A. 1981. Hot mechanical properties of 316L stainless steel with boron and nitrogen additions. Mechanical Behavior and Nuclear Applications of Stainless Steel at elevated-temperatures, The Metals Society, London, England, pp. 39–46.

9. Roberts, A. C., and Evans, H. E. 1981. Effects of titanium and silicon additions on creep behavior of TiN-dispersion-strengthened 20Cr-25Ni stainless steel. Mechanical Behavior and Nuclear Applications of Stainless Steel at elevated-temperatures, The Metals Society, London, England, pp. 51–57.

10. Grover, H. K., and Wickens, A. 1981. Effects of minor elements on long-term creep rupture properties of 316 austenitic stainless steel at SS0°–700°C. Mechanical Behavior and Nuclear Applications of Stainless Steel at elevated-temperatures, The Metals Society, London, England, pp. 81–87.

11. Vitek, J. M., and David, S. A. 1984. The solidification and aging behavior of Types 308 and 308CRE stainless steel welds. *Welding Journal* 63(8): 246-s to 253-s.

12. David, S. A., Goodwin, G. M., and Braski, D. N. 1979. Solidification behavior of austenitic stainless steel filler metals. *Welding Journal* 58(11): 330-s to 336-s.

13. Vitek, J. M., and David, S. A. 1987. The aging behavior of homogenized Types 308 and 308CRE stainless steel. *Metall. Trans. A* 18A(7):1195–1201.

14. Hull, F. C. 1973. Delta ferrite and martensite formation in stainless steels. *Welding Journal* 52(5): 193-s to 203-s.

15. AWS Standard A4.2-74, 1974. *Standard Procedures for Calibrating Magnetic Instruments to Measure the Delta Ferrite Content of Austenitic Stainless Steel Weld Metal.* American Welding Society, Miami, Fla.

16. Vitek, J. M., and Klueh, R. L. 1983. Precipitation reactions during the heat treatment of ferritic steels. *Metall. Trans. A* 18A:1047–1055.

17. David, S. A. 1981. Ferrite morphology and variations in ferrite content in austenitic stainless steel welds. *Welding Journal* 60(4):63-s to 71-s.

18. Vitek, J. M., and David, S. A. 1987. Time-dependent composition behavior of precipitates in aged stainless steels. *Analytical Electron Microscopy* — 1987, D. C. Joy, ed., San Francisco Press, San Francisco, Calif., pp. 21–24.

19. Vitek, J. M., and David, S. A. 1985. Metastable equilibrium of ferrite in Type 308 stainless steel. *Scripta Metall.* 19:23–26.

20. Lai, J. K., and Haigh, J. R. 1979. Delta ferrite transformations in a Type 316 weld metal. *Welding Journal* 58(1):1-s to 6-s.

21. Dean, M. S., and Plumbridge, W. J. 1981. Aging of Type 316 stainless steel and its effect on creep and fatigue behavior. Mechanical Behavior and Nuclear Applications of Stainless Steel at elevated temperatures, The Metals Society, London, England, pp. 73–80.

22. Haigh, J. R. 1977. Creep crack growth in a Type 316 stainless steel weld metal. *Welding Journal* 56(5):149-s to 153-s.

23. Thomas, R. G., Nicholson, R. D., and Farrar, R. A. 1984. Creep-rupture properties and microstructure of AISI Type 316L submerged arc weld metals. *Metals Technol.* 11:61–65.

24. Vitek, J. M., and David, S. A. 1986. The sigma phase transformation in austenitic stainless steels. *Welding Journal* 65(4): 106-s to 111-s.

WRC Bulletin 366
August 1991

Recommended Practices in Elevated Temperature Design: A Compendium of Breeder Reactor Experiences (1970–1987), Volume IV — Special Topics

Edited by A. K. Dhalla

The recommended practices for elevated temperature design of Liquid Metal Fast Breeder Reactors (LMFBR) has been consolidated into four volumes and is published in four individual WRC Bulletins.

Volume I — Current Status and Future Directions, in WRC Bulletin 362, April 1991
Volume II — Preliminary Design and Simplified Methods, in WRC Bulletin 363, May 1991
Volume III — Inelastic Analysis, in WRC Bulletin 365, July 1991
Volume IV — Special Topics, in WRC Bulletin 366, August 1991

In Volume IV, WRC Bulletin 366, special topics such as, fracture mechanics, nonlinear collapse stress classification of structural discontinuity stresses, and high-temperature design as practiced in Germany are discussed. Flaw evaluation (fracture mechanics) procedures are recommended to supplement the design codes which assume perfect, defect-free structures. The fracture mechanics methods have been extended into the plastic and creep regimes.

Publication of this Bulletin was sponsored by the Committee on Elevated Temperature of the Pressure Vessel Research Council. The price of WRC Bulletin 366 is $40.00 per copy, plus $5.00 for U.S. and $10.00 for overseas, postage and handling. Orders should be sent with payment to the Welding Research Council, Room 1301, 345 E. 47th St., New York, NY 10017.

WRC Bulletin 367
September 1991

Basis of Current Dynamic Stress Criteria for Piping

By G. C. Slagis

The evolution and development of the ASME Boiler and Pressure Vessel Code requirements for seismic design of piping are documented. The development of analytical methods and regulatory requirements for seismic design are reviewed.

Publication of this report was sponsored by the Pressure Vessel Research Council of the Welding Research Council, Inc. The price of WRC Bulletin 367 is $40.00 per copy, plus $5.00 for U.S. and $10.00 for overseas, postage and handling. Orders should be sent with payment to the Welding Research Council, Room 1301, 345 E. 47th St., New York, NY 10017.

WRC Bulletin 361
February 1991

This Bulletin contains two reports that compare the French RCC-M Pressure Vessel Code and the U.S ASME Section III Code on Design of Nuclear Components and Piping Design Rules.

(1) Improvements on Fatigue Analysis Methods for the Design of Nuclear Components Subjected to the French RCC-M Code

By J. M. Grandemange, J. Heliot, J.Vagner, A. Morel and C. Faidy

(2) Framatome View on the Comparison between Class 1 and Class 2 RCC-M Piping Design Rules

By C. Heng and J. M. Grandemange.

Publication of this bulletin was sponsored by the Pressure Vessel Research Council of the Welding Research Council. The price of WRC Bulletin 361 is $30.00 per copy, plus $5.00 for U.S. and $10.00 for overseas, postage and handling. Orders should be sent with payment to the Welding Research Council, Room 1301, 345 E. 47th St., New York, NY 10017.

WRC Bulletin 362
April 1991

Recommended Practices in Elevated-Temperature Design: A Compendium of Breeder Reactor Experiences (1970–1987), Volume I—Current Status and Future Directions

Edited by A. K. Dhalla

The recommended practices for elevated-temperature design of liquid metal fast breeder reactors (LMFBR) have been consolidated into four volumes to be published in four individual WRC bulletins.

Volume I: Current Status and Future Directions (WRC Bulletin 362)
Volume II: Preliminary Design and Simplified Methods (WRC Bulletin (363)
Volume III: Inelastic Analysis (WRC Bulletin 365)
Volume IV: Special Topics (WRC Bulletin 366)

Volume I presents the current status of the international design codes and structural technology for LMFBR's. Structural components designed by various countries that were found to be successful for long-term elevated-temperature operation are included.

Publication of this bulletin was sponsored by the Committee on Elevated Temperature Design of the Pressure Vessel Research Council. The price of WRC Bulletin 362 is $45.00 per copy, plus $5.00 for U.S. and $10.00 for overseas, postage and handling. Orders should be sent with payment to the Welding Research Council, Room 1301, 345 E. 47th St., New York, NY 10017.